Virologica Sinica 39 (2024) 144–155

Contents lists available at ScienceDirect

Virologica Sinica

journal homepage: www.keaipublishing.com/en/journals/virologica-sinica
www.virosin.org

Research Article

Ferroptosis contributes to JEV-induced neuronal damage and neuroinflammation

Wenjing Zhu [a,b,c,d], Qi Li [a,b,c,d], Yong Yin [a,b,c,d], Huanchun Chen [a,b,c,d], Youhui Si [a,b,c,d], Bibo Zhu [a,b,c,d], Shengbo Cao [a,b,c,d], Zikai Zhao [a,b,c,d,*], Jing Ye [a,b,c,d,*]

[a] National Key Laboratory of Agricultural Microbiology, Huazhong Agricultural University, Wuhan, 430070, China
[b] Frontiers Science Center for Animal Breeding and Sustainable Production, Huazhong Agricultural University, Wuhan, 430070, China
[c] The Cooperative Innovation Center for Sustainable Pig Production, Huazhong Agricultural University, Wuhan, 430070, China
[d] Hubei Hongshan Laboratory, Wuhan, 430070, China

ARTICLE INFO

Keywords:
Japanese encephalitis virus (JEV)
Ferroptosis
Neuron
Lipid peroxidation
Inflammatory response

ABSTRACT

Ferroptosis is a newly discovered prototype of programmed cell death (PCD) driven by iron-dependent phospholipid peroxidation accumulation, and it has been linked to numerous organ injuries and degenerative pathologies. Although studies have shown that a variety of cell death processes contribute to JEV-induced neuroinflammation and neuronal injury, there is currently limited research on the specific involvement of ferroptosis. In this study, we explored the neuronal ferroptosis induced by JEV infection *in vitro* and *in vivo*. Our results indicated that JEV infection induces neuronal ferroptosis through inhibiting the function of the antioxidant system mediated by glutathione (GSH)/glutathione peroxidase 4 (GPX4), as well as by promoting lipid peroxidation mediated by yes-associated protein 1 (YAP1)/long-chain acyl-CoA synthetase 4 (ACSL4). Further analyses revealed that JEV E and prM proteins function as agonists, inducing ferroptosis. Moreover, we found that treatment with a ferroptosis inhibitor in JEV-infected mice reduces the viral titers and inflammation in the mouse brains, ultimately improving the survival rate of infected mice. In conclusion, our study unveils a critical role of ferroptosis in the pathogenesis of JEV, providing new ideas for the prevention and treatment of viral encephalitis.

1. Introduction

Japanese encephalitis virus (JEV), a member of the genus *Flavivirus* in the *Flaviviridae* family, is a serious zoonotic pathogen transmitted primarily by mosquito. JEV is the leading cause of viral encephalitis in humans. Annually, 68,000 clinical cases are recorded, with 25%–30% mortality and 30%–50% survivors suffering long-term neurological or psychiatric aftereffects (Khare and Kuhn, 2022). Inducing neuronal cell death and excessive neuroinflammation are the key factors in the pathogenesis of JEV, but the molecular mechanisms are poorly understood.

Ferroptosis is a newly discovered programmed cell death (PCD) driven by iron-dependent phospholipid peroxide (Dixon et al., 2012). This unique form of cell death has been well proven to be regulated by various cellular metabolic events, and morphologically characterized by mitochondrial atrophy, decreased mitochondrial cristae, and altered phospholipid bimolecular structure and membrane fluidity, which is obviously different from other PCDs (Cao and Dixon, 2016; Stockwell et al., 2017). In addition to this, there is a significant accumulation of Fe^{2+} and lipid peroxidation in the cells where ferroptosis occurs (Yuan et al., 2021). Specifically, excessive intracellular accumulation of Fe^{2+} tends to undergo the Fenton reaction, resulting in excessive production of reactive oxygen species (ROS), which subsequently catalyze the lipid peroxidation of polyunsaturated fatty acids (PUFAs) in the cell membrane, leading to cell membrane damage (Dixon et al., 2012; Tang et al., 2021).

Ferroptosis is tightly regulated by intracellular signaling pathways, including the regulatory pathway of iron homeostasis, the transport pathway of cystine, and the synthesis pathway of fatty acids. Among them, dysregulation of the glutathione peroxidase 4 (GPX4)-mediated antioxidant system is thought to be one of the main causes of ferroptosis, and loss of GPX4 function leads to excessive accumulation of phospholipid hydroperoxides and triggers catalytic reactions in the presence of transition metals (e.g., iron), ultimately leading to cell death (Tang et al., 2021; Zhang et al., 2023). Meanwhile, glutathione (GSH) depletion leads to GPX4 inactivation as it serves as an electron donor for the reduction of toxic phospholipid hydroperoxides to nontoxic phospholipid alcohols,

* Corresponding authors.
E-mail addresses: zkzhao@mail.hzau.edu.cn (Z. Zhao), yej@mail.hzau.edu.cn (J. Ye).

https://doi.org/10.1016/j.virs.2023.12.004
Received 13 May 2023; Accepted 13 December 2023
Available online 15 December 2023

and oxidized glutathione (GSSG) is produced as a byproduct during this process (Yang et al., 2014; Forcina and Dixon, 2019). In addition, Acyl-CoA synthase long chain family member 4 (ACSL4) is also an important component of ferroptosis execution. ACSL4 catalyzes the synthesis of polyunsaturated fatty acids (PUFAs), the substrate for lipid peroxidation, thereby promoting lipid peroxidation and causing cell death (Yuan et al., 2016; Doll et al., 2017).

Recently, studies have demonstrated that ferroptosis is involved in the pathogenesis of various viruses. For example, Hepatitis B virus protein X stabilizes enhancer of zeste homolog 2 (EZH2) and promotes trimethylation of H3K27, which inhibits SLC7A11 and induces ferroptosis in acute liver failure (Liu et al., 2021). HSV-1 disrupts cellular redox homeostasis and promotes ferroptosis by enhancing keap1-dependent ubiquitination and degradation of nuclear factor erythroid 2-related factor 2 (Nrf2) (Xu et al., 2022). Newcastle disease virus (NDV) induces GPX4-dependent ferroptosis by activating p53 (Kan et al., 2021). Although a recent study using RNA-seq has demonstrated that ferroptosis-related pathways are significantly activated in ZIKV-infected mouse brains (Yan et al., 2023), there is still no clear evidence on whether ferroptosis is involved in the pathogenesis of flaviviruses.

Here, we showed that JEV infection leads to neuronal ferroptosis by inhibiting the function of GPX4 and upregulating the expression of ACSL4, resulting in the neuronal damage and an inflammation response. By establishing a mouse model, we further revealed that inhibition of ferroptosis reduces the mortality, and alleviates the neuroinflammation response and the cerebral damage caused by JEV infection. This study provides novel insights into the mechanism of JEV-induced neuronal cell death, and may provide new ideas for the prevention and treatment of viral encephalitis.

2. Materials and methods

2.1. Reagents and antibodies

Ferroptosis agonist (Erastin, S7242), ferroptosis inhibitors [Liproxstatin-1 (Lip-1), S7699], co-solvents (PEG300, S6704) and Tween 80 (S6702) were purchased from Selleck (Shanghai, China).

Mouse monoclonal anti-JEV NS5 and anti-JEV E antibodies were prepared in our laboratory. GPX4 (A11243), ACSL4 (A20414), YAP1 (A21216) and GAPDH (AC002) antibodies were purchased from Abclonal Technology (Wuhan, China), and goat anti-mouse/rabbit secondary antibody labeled by horseradish peroxidase was purchased from Bosterbio (Wuhan, China).

2.2. Cells and viruses

BHK-21 cells (hamster kidney cell line), HeLa cells (human cervical cancer cell line), BV2 cells, HEK-293T cells (human microglia cell line) were cultured in Dulbecco's modified Eagle's medium (DMEM, Sigma) with 10% fetal bovine serum (FBS), 100 U/mL penicillin and 100 mg/mL streptomycin sulfate in a 37 °C, 5% CO_2 incubator. SH-SY5Y cells (human neuroblastoma cell line) were cultured in Dulbecco's modified Eagle's medium (DMEM/High Glucose) and F12 (Servicebio) (1:1) medium with 10% FBS, 100 U/mL penicillin, and 100 mg/mL streptomycin sulfate in a 37 °C, 5% CO_2 incubator.

The JEV P3 strain was stored in our laboratory. Cells were infected with JEV at an MOI of 1 for 1 h, followed by removal of the supernatant and addition of maintenance medium containing 3% FBS. For the use of inhibitors, Lip-1 was added into maintenance medium at a concentration of 20 μmol/L, and maintained throughout the experiment.

2.3. Cell viability assay

For the cell viability assay, cells were seeded in 96-well plates with 50,000 cells per well, treated with JEV, Lip-1, and Ethanol and detected using the CellTiter-Glo Luminescent Cell Viability Assay kit (Promega, G7570). NC cell lines, ACSL4 KD cell lines and YAP1 KD cell lines were seeded in 96-well plates with 50,000 cells per well, and the cell viability of each cell line was determined after 48 h using the CellTiter-Glo Luminescent Cell Viability Assay kit (Promega, G7570).

2.4. UV inactivation of JEV

JEV stock solution was placed in a sterile 35 mm culture dish. The exposed virus was irradiated with one 30W UV-C lamp, which was placed 5 cm above the surface of the medium, with a radiation peak at 253.7 nm for 30 min. Inactivation was verified through plaque assay and RT-qPCR.

2.5. Western blotting

Total cell lysates were prepared using the RIPA buffer (Sigma) containing protease inhibitors (Roche). After sonication, the protein concentration in each sample was determined by using the BCA protein assay kit (Thermo Fisher Scientific) and boiled at 95 °C for 10 min. Equivalent amounts of protein samples were separated by SDS-PAGE and electroblotted onto a polyvinylidene fluoride membrane (Roche) using a Mini Trans-Blot Cell (Bio-Rad). The membranes were blocked at room temperature (RT) for 2 h in PBS containing 3% bovine serum albumin (BSA), followed by incubation with the indicated primary antibodies overnight at 4 °C. After washing three times with TBS-Tween (50 mmol/L Tris-HCl, 150 mmol/L NaCl, and 0.1% [v/v] Tween 20, pH 7.4), the membranes were incubated with secondary antibodies at room temperature for 45 min. Finally, the membranes were visualized with a chemiluminescence system (Bio-Rad) after three times of wash.

2.6. RNA extraction and quantitative Real-time PCR (RT-qPCR)

Total RNA from cells was extracted using Trizol reagent (Invitrogen) and cDNA was synthesized with 1 μg of RNA using ABscriptII cDNA First Strand synthesis kit (ABclonal Technology). RT-qPCR was performed using the 2× Universal SYBR Green Fast qPCR Mix (Abclonal Technology) in the 7500 Real-Time PCR System (Applied Biosystems). The data were normalized to the level of *ACTB* or *Actb* expression in each sample. The primers used in RT-qPCR are listed in Supplementary Table S1.

2.7. Plaque assay

The harvested cell supernatants were serially diluted with DMEM, inoculated into a monolayer of BHK-21 cells at 37 °C, discarded for 1 h and washed three times with DMEM, switched to sodium carboxymethylcellulose (Sigma) containing 3% FBS for 4 days. Finally, after 10% formaldehyde fixation and crystal violet staining, the virus titer was calculated according to the visible plaques.

2.8. Lipid peroxidation assay and MDA assay

Intracellular lipid peroxidation was detected using BODIPY™ 581/591 C11 (Invitrogen). The cells were seeded in 6-well plates in advance, and after viral infection or drug treatment according to experimental needs, the medium was discarded and washed once with PBS, and after 30 min incubation with 7 μmol/L C11 BODIPY 581/591, the cells were collected by trypsinization, and lipid peroxidation was detected by a flow cytometer 488 nm laser FL1 detector after centrifugation and PBS washing. Mouse brain tissue MDA (lipid peroxidation product) was detected using the Lipid Peroxidation MDA Assay Kit (Beyotime), and the specific steps were tested according to the manufacturer's instructions.

2.9. GSH assay

Cells are seeded in 12-well plates, collected after viral infection or drug treatment, and tested according to the instructions for the GSH and

GSSG Assay Kit (Beyotime). GSH and GSSG concentrations were calculated using a standard curve and normalize to total protein levels.

2.10. CRISPR-Cas9 KD cells

The CRISPR-Cas9 expression system using single-guide RNAs (sgRNAs) knocks down ACSL4 or YAP1 in cells. First, sgRNA was cloned onto lentiGuide vectors, and HEK-293T cells were co-transfected with packaged plasmids pMD2.G and pSPAX2 using FuGENE HD Transfection Reagent (Promega). After 48 h, viral supernatants were collected to infect SH-SY5Y cells and sgRNA-expressing cells were screened out with 1 μg/mL puromycin.

The sequences of sgRNAs were as follows:

ACSL4 sgRNA: 5′- CACCGCGTGTGCATCGTCACCAACG -3′

YAP1 sgRNA: 5′- CACCG GAGGCAGAAGCCATGGATCC -3′

2.11. Construction of JEV structural protein stable ectopic expressed SH-SY5Y cell lines

Using the JEV cDNA as template, *C*, *prM*, and *E* genes were separately cloned into the p3×FLAG-CMV-10 using the PCR/restriction digest-based cloning method, and were verified by sequencing. Then the target genes with 3× flag tag at the N-terminus were ligated into the pLV-EF1α-IRES-Puro lentiviral vector through ClonExpress Ultra One Step Cloning Kit V2 (Vazyme). For stable expression, the pLV-EF1α-IRES-Puro lentiviral vector containing the desired gene, together with the packing plasmids pMD2.G and pSPAX2, were transfected into HEK-293T cells. At 48 h post-transfection, viral supernatants were collected, and then inoculated to SH-SY5Y cells for another 48 h. The infected cells were selected with 1 μg/mL puromycin, and then plated into 12-well plates for further experiments.

2.12. Animal experiments

Adult five-week-old C57BL/6 mice were purchased from the Laboratory Animal Center, Huazhong Agricultural University, Wuhan, China. Mice were randomly divided into four groups: a control group (Mock + DMSO; n = 13); a group treated with Lip-1 alone (Mock + Lip-1; n = 13); JEV and cosolvent treatment group (JEV + DMSO; n = 13); JEV and Lip-1 treatment groups (JEV + Lip-1; n = 13). Mice in the JEV-infected group were Intravenous injected with 10^5 PFU JEV P3 strain, while the mock group was treated with DMEM. Lip-1 was administered via intravenous injection at a dose of 10 mg/kg per mouse, and the control group was treated with co-solvent.

2.13. Hematoxylin-eosin (H&E) staining and immunohistochemistry

Brain tissue samples were collected and sectioned after title wax block, and the sections were stained by H&E staining and examined by IHC, respectively. Antibodies used for IHC are as follows: anti-IBA-1, anti-GFAP and anti-NEUN. IHC was analyzed using ImageJ software.

2.14. Isolation of mouse primary neurons and glial cells

C57BL/6 mice were set up for timed matings, and whole brains were extracted from embryos at embryonic day 15–16. In aseptically conditions, cerebral cortex from embryos were gently separated from the brain in pre-cooling HBSS solution (Sigma). Isolated cortex hemispheres were then cut into small pieces (~1 mm^3) and treated with 0.25% Trypsin for 15–20 min at 37 °C to perform enzymatic dissociation. Then transfer the enzymatically digested tissue to DMEM containing 5% FBS (Gibco) and 0.75 mg/mL Dnase I (Beyotime Biotechnology), continue to react at 37 °C for another 5 min. After gently resuspend, the obtained cell suspension was placed on ice and allowed to stand for 5 min. Then the supernatant was transferred to a new centrifuge tube, and centrifuged at 1000 ×*g* for 3 min to obtain primary cells. The primary cells were collected and diluted to 5×10^6 cells/mL and maintained in DMEM medium containing 5% FBS. The mixed primary cells were seeded in polylysine-coated (20 mg/mL, Beyotime Biotechnology) 12-well plates, and replaced culture medium with Neurobasal medium (Gibco) supplemented with 2% B-27 (Gibco) at 6 h post-seeding, and cultured for 4 days to obtain primary neurons for subsequent experiments. To obtain primary glial cells, the obtained mixed primary cells were seeded in 12-well plates, and the culture medium was replaced with DMEM containing 10% FBS at 24 h post-seeding. The cells were then cultured for 7–10 days.

2.15. Statistical analysis

All experiments were conducted at least three times with similar results. Statistical analysis was carried out using GraphPad Prism software (version 8.0.1) for Student's two-tailed unpaired *t*-test for both groups or Dunnett's multiple comparison test for one-way ANOVA.

3. Results

3.1. JEV infection induces ferroptosis in neurons

Although it has been reported that JEV infection can reduce intracellular GSH concentration and the activity of GPX4 in mouse brain (Kumar et al., 2009), whether ferroptosis is involved in the pathogenesis of JEV remains to be further studied. We first explored whether JEV infection can regulate the expression of ferroptosis-related genes in neurons. As shown in Fig. 1A–B and Supplementary Fig. S1A–D, both ferroptosis agonist treatment or JEV infection significantly increased the expression of *PTGS2*, which was considered as a marker of ferroptosis (Zhou et al., 2022), in SH-SY5Y cells and mouse primary neurons. We then observed JEV-infected SH-SY5Y cells through electron microscopy, and found typical ferroptosis-related morphological abnormalities, including mitochondrial shrinkage, reduction of mitochondrial cristae, and mitochondrial outer membrane rupture, which are consistent with previous reports (Fig. 1C) (Yagoda et al., 2007; Dixon et al., 2012; Friedmann Angeli et al., 2014). Since ferroptosis is driven by lethal lipid peroxidation, we then detected the level of lipid peroxidation in JEV-infected cells. The results showed that, similar to the ferroptosis agonist-treated group (Supplementary Fig. S1E and F), JEV infection significantly promoted lipid peroxidation in SH-SY5Y cells and mouse primary neurons in a time-dependent manner (Fig. 1D–G). These findings suggested that JEV infection may lead to neuronal ferroptosis. To further clarify this conclusion, ferroptosis inhibitor Lip-1 was employed to test whether inhibiting ferroptosis could affect neuronal death induced by JEV infection. It was found that Lip-1 treatment not only reduced the level of lipid peroxidation in JEV-infected SH-SY5Y cells, but also inhibited the cell death caused by JEV infection (Fig. 1H–J). Overall, these findings demonstrate that JEV infection induces the ferroptosis in neurons.

In order to determine whether JEV-induced ferroptosis is specifically in neurons, experiments were conducted on HeLa, BHK-21 and BV2 cells, and the results showed that JEV could induce ferroptosis in BHK-21 cells but not in HeLa and BV2 cells (Supplementary Fig. S2), suggesting that JEV-induced ferroptosis is not a common cellular process during infection. However, further investigation is necessary to determine the underlying factors that govern the occurrence of ferroptosis in JEV-infected cells.

3.2. JEV infection inhibits GSH-GPX4 pathway

It is known that GPX4-mediated scavenging of lipid peroxides plays a central role in regulating ferroptosis, and relevant studies have shown that JEV can inhibit the activity of GPX4 (Kumar et al., 2009). Hence, we

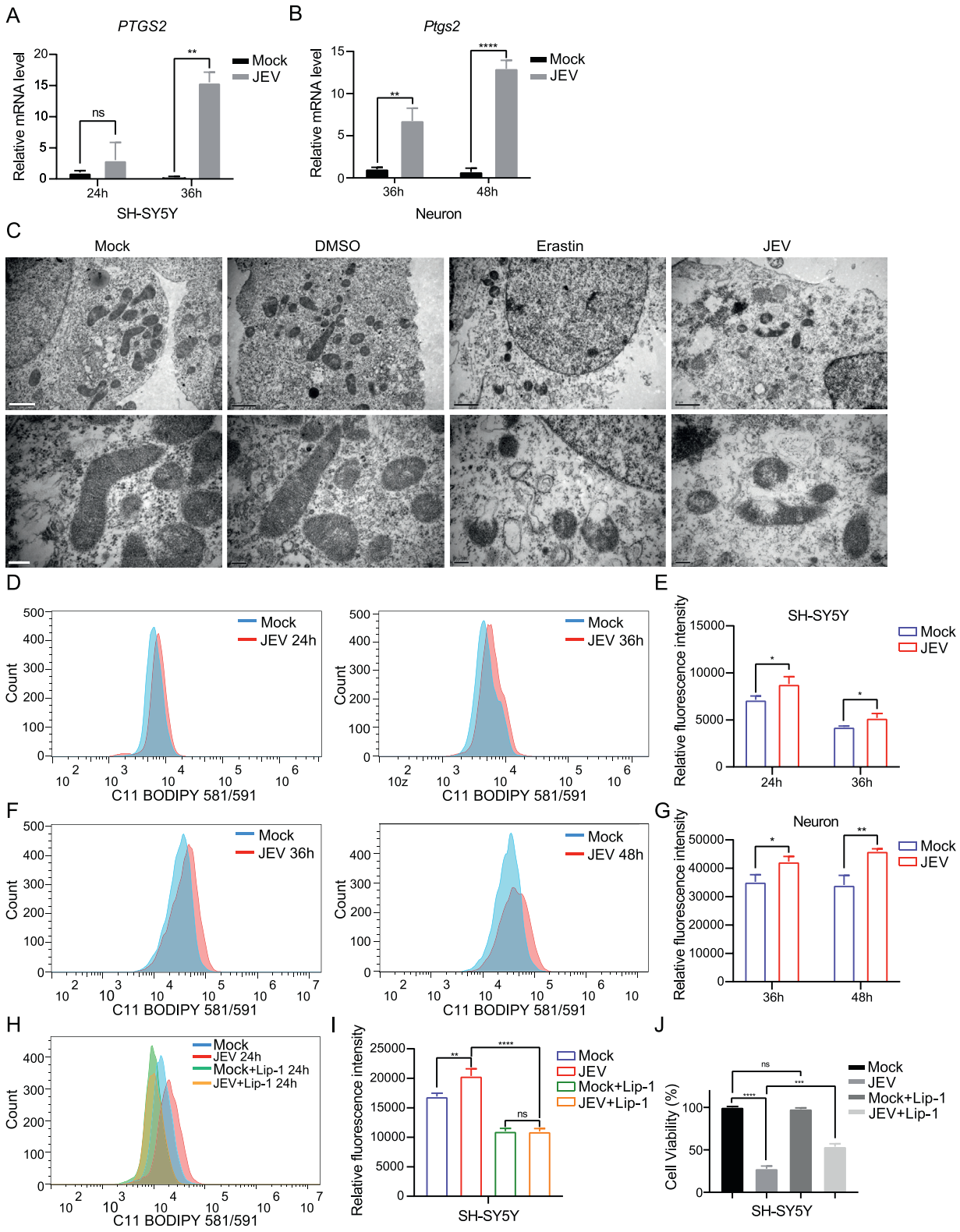

Fig. 1. JEV infection induces ferroptosis in neurons. **A** and **B** SH-SY5Y cells or mouse primary neurons were infected with JEV at an MOI of 1 or mock-infected. At indicated time post-infection, cells were subjected to RT-qPCR to detect the mRNA level of *PTGS2*. **C** Transmission electron microscopy of SH-SY5Y cells treated with DMSO (12 h), erastin (10 μmol/L, 12 h), and JEV (1 MOI, 24 h). Scale bars, 1 μm (top row), 200 nm (bottom row). **D** to **G** SH-SY5Y cells or mouse primary neurons were infected with JEV at an MOI of 1 or mock-infected. At indicated time post-infection, cells were harvested and stained with C11 BOIPY 581/591, followed by analysis of lipid peroxidation through flow cytometry. **H** to **J** SH-SY5Y cells were infected with JEV at an MOI of 1 or mock-infected, followed by incubated with 20 μmol/L Lip-1 or the vehicle (Ethanol). At 24 h post-infection, the cells were subjected to detect the level of lipid peroxidation (H and I), and the cell viability (**J**). Data are representative of three independent experiments with three biological replicates. Significance was analyzed using a Student's two-tailed unpaired *t*-test (n = 3 in each group). $^{*}P < 0.05$, $^{**}P < 0.01$, $^{***}P < 0.001$, $^{****}P < 0.0001$. ns, not significant.

explored the role of the GPX4-mediated antioxidant pathway in response to JEV infection. As shown in Fig. 2A–C, JEV infection decreased the content of intracellular GSH, and inhibited the expression of GPX4 in SH-SY5Y cells. Moreover, GPX4-overexpressed and GPX4 knockdown (KD) SH-SY5Y cells were generated respectively (Fig. 2D and Supplementary Fig. S3A and B), followed by infection with JEV at an MOI of 1. As expected, overexpression of GPX4 abolished the upregulation of lipid peroxidation induced by JEV infection (Fig. 2E and F), while KD of GPX4 remarkably promoted this process (Supplementary Fig. S3C and D). Taken together, the results indicate that JEV infection induces ferroptosis in neurons by inhibiting the function of GSH-GPX4 axis.

3.3. JEV induces ferroptosis by affecting the YAP1-ACSL4 pathway

Long-chain acyl-CoA synthetase 4 (ACSL4) is essential for the occurrence of ferroptosis, which catalyzes the biosynthesis of lipid containing PFUAs and promotes the accumulation of lipid peroxidation products (Zhang et al., 2022). Mechanistically, ACSL4 activates PUFAs, which are then inserted into plasma membrane phospholipids via lysophosphatidylcholine acyltransferase 3 (LPCAT3) (Yuan et al., 2016; Doll et al., 2017). Arachidonic acid (C20:4) and adrenic acid (C22:4) are the main lipid peroxidation substrates that contribute to the occurrence of ferroptosis (Doll et al., 2017; Kagan et al., 2017; Lee et al., 2020). Therefore, we subsequently explored the effect of JEV infection on ACSL4 and its upstream key transcriptional activator YAP1 (Wu et al., 2019; Yang et al., 2020; Chen et al., 2022). As shown in Fig. 3A–F, JEV infection significantly promoted the expression of yes-associated protein 1 (YAP1) and ACSL4 at the protein and mRNA levels in SH-SY5Y cells, implying that JEV may induce ferroptosis by affecting their functions. To test this hypothesis, we generated ACSL4 KD SH-SY5Y cells (Fig. 3G), and cell viability assays showed that KD of ACSL4 had no effect on cells (Fig. 3H). JEV infection of ACSL4 KD or wild-type cells revealed that KD of ACSL4 conspicuously attenuated the JEV-induced lipid peroxidation (Fig. 3I and J). We subsequently generated YAP1 KD SH-SY5Y cells to verify its function in JEV-induced ferroptosis (Fig. 3K and L). It was found that KD of YAP1 abrogated the upregulation of ACSL4 and lipid peroxidation induced by JEV infection (Fig. 3M–P), indicating that JEV infection promoted ASCL4-mediated ferroptosis by up-regulating the expression of YAP1. Collectively, our results demonstrate that the YAP1/ACSL4 axis play an important role in JEV-induced neuronal ferroptosis.

3.4. JEV E and prM proteins contribute to ferroptosis

In order to explore which component of JEV is responsible for inducing ferroptosis, we infected SH-SY5Y cells with JEV and UV-inactivated JEV(UV), and collected cell supernatants and cells at different time points for the detection of ferroptosis (Fig. 4A). The results showed that JEV(UV) still induced the upregulation of *PTGS2* (Fig. 4B), degradation of GPX4 (Fig. 4C and D), and promotion of lipid peroxidation in SH-SY5Y cells (Fig. 4E and F), indicating that JEV-induced neurons ferroptosis may be attributed to structural proteins.

For the purpose of elucidating which JEV structural protein works as a ferroptosis agonist during infection, three FLAG-tagged structural proteins of JEV were ectopic expressed in SH-SY5Y cells respectively. As shown in Fig. 4G–J, ectopic expression of JEV E or prM remarkably led to the degradation of GPX4 and the upregulation of *PTGS2* and lipid peroxidation, while ectopic expression of JEV C had no noticeable effect. Thereby, these data indicate that JEV E and prM proteins contribute to ferroptosis during infection.

3.5. Ferroptosis contributes to JEV-induced neuroinflammatory response in vitro

Given the important role of ferroptosis in inflammation, we sought to investigate whether JEV-induced neuronal ferroptosis is associated with neuroinflammation caused by JEV infection. To this end, mouse primary neurons were isolated and infected with JEV, and the infected cells and the supernatant were collected at 48 h post-infection. The RT-qPCR analysis revealed that JEV infection significantly increased the production of inflammatory cytokines, and this process was partially prevented in the presence of ferroptosis inhibitor Lip-1 (Fig. 5A and B).

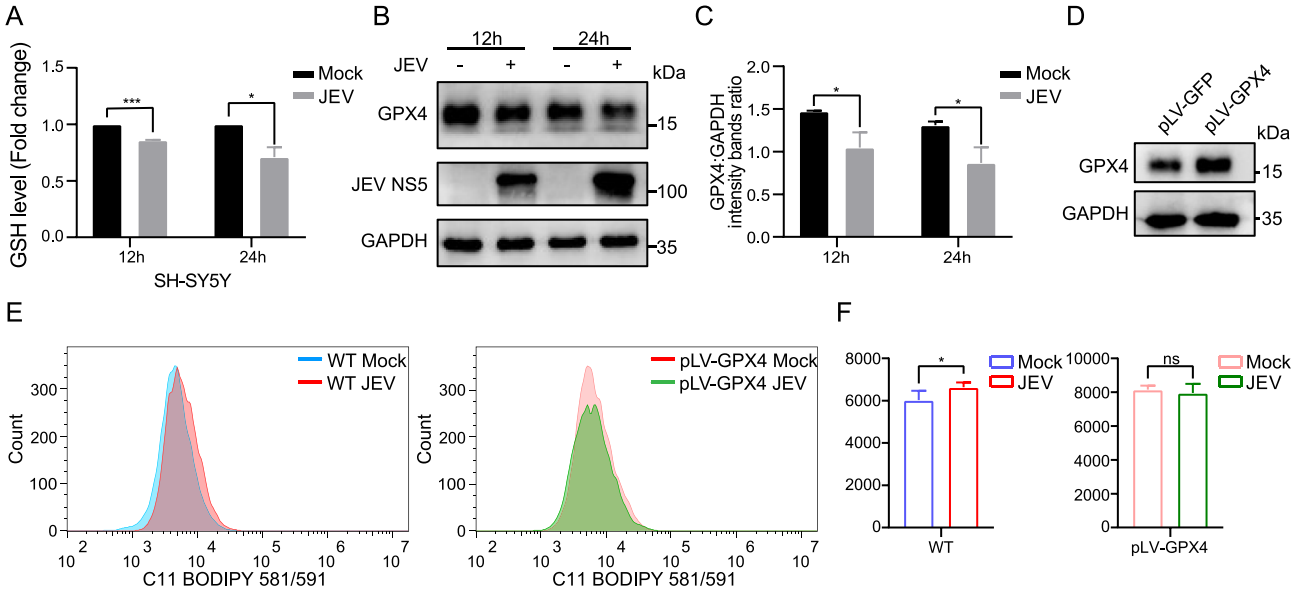

Fig. 2. JEV infection inhibits GSH-GPX4 pathway. **A** to **C** SH-SY5Y cells were infected with JEV at an MOI of 1 or mock-infected. At indicated time post-infection, cells were harvested and the intracellular GSH levels were measured using a GSSG/GSH quantification kit (**A**). Total proteins were subjected to Western blotting analysis for detecting the expression of GPX4 and JEV NS5 (**B**). Relative quantification of GPX4, normalized by GAPDH, was performed using ImageJ software (**C**). **D** Western blotting analysis of the expression of GPX4 in SH-SY5Y cells. **E** and **F** Wild type (WT) and pLV-GPX4 cells were infected with JEV at an MOI of 1 or mock-infected. At indicated time post-infection, cells were harvested and stained with C11 BOIPY 581/591, followed by analysis of lipid peroxidation through flow cytometry. Data are representative of three independent experiments with three biological replicates. Significance was analyzed using a Student's two-tailed unpaired *t*-test (**A**, **C** and **F**) (n = 3 in each group), $^{*}P < 0.05$, $^{**}P < 0.01$, $^{***}P < 0.001$. ns, not significant.

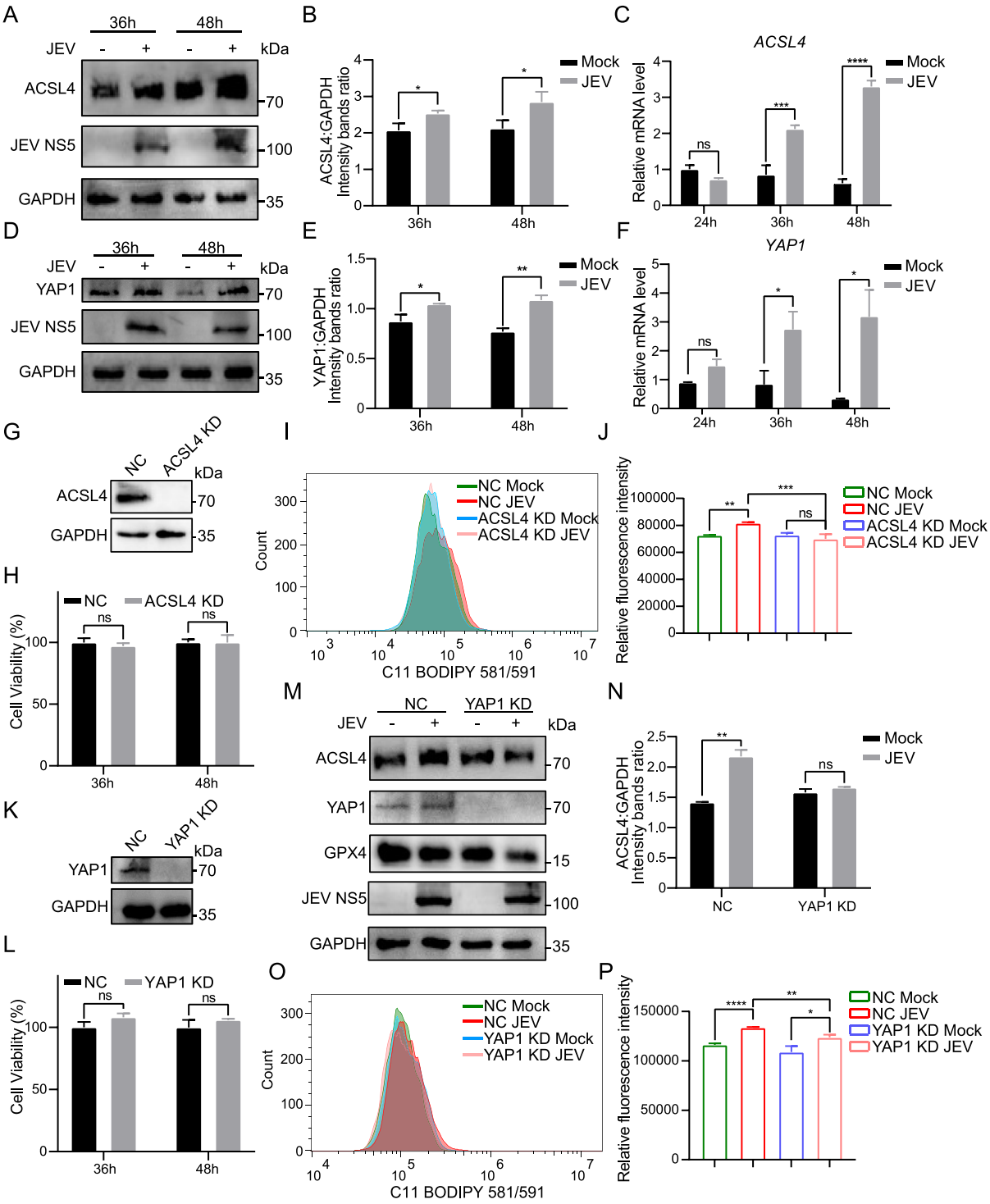

Fig. 3. JEV induces ferroptosis by affecting the YAP1-ACSL4 pathway. **A** to **F** SH-SY5Y cells were infected or mock-infected with JEV at an MOI of 1. At indicated time post-infection, cells were harvested and subjected to Western blotting analysis for detecting the expression of ACSL4, YAP1 and JEV NS5 (**A** and **D**). Relative quantification of ACSL4 and YAP1 normalized by GAPDH were performed using ImageJ software (**B** and **E**). Total RNAs were extracted from the cells from different groups and subjected to RT-qPCR to detect the mRNA levels of *YAP1* and *ACSL4* (**C** and **F**). **G** and **H** ACSL4 knockdown (KD) cells were subjected to Western blotting analysis for detecting the expression of ACSL4 (**G**) and the viability assay at different time (**H**). **I** and **J** NC and ACSL4 KD cells were infected or mock-infected with JEV at an MOI of 1. At 24 h post-infection, the cells were subjected to detect the level of lipid peroxidation. **K** and **L** YAP1 KD cells were subjected to Western blotting analysis of the expression of YAP1 (**K**) and the viability assay at different time (**L**). **M** and **N** NC and YAP1 KD cells were infected with JEV at an MOI of 1. At 36 h post-infection, total proteins were subjected to Western blotting analysis for detecting the expression of ACSL4, YAP1, GPX4 and JEV NS5 (**M**). Relative quantification of ACSL4 normalized by GAPDH was performed using ImageJ software (**N**). **O** and **P** NC and YAP1 KD cells were infected or mock-infected with JEV at an MOI of 1. At 24 h post-infection, the cells were subjected to detect the level of lipid peroxidation. Data are representative of three independent experiments with three biological replicates. Significance was analyzed using a Student's two-tailed unpaired *t*-test (n = 3 in each group). $^{*}P < 0.05$, $^{**}P < 0.01$, $^{***}P < 0.001$, $^{****}P < 0.0001$. ns, not significant.

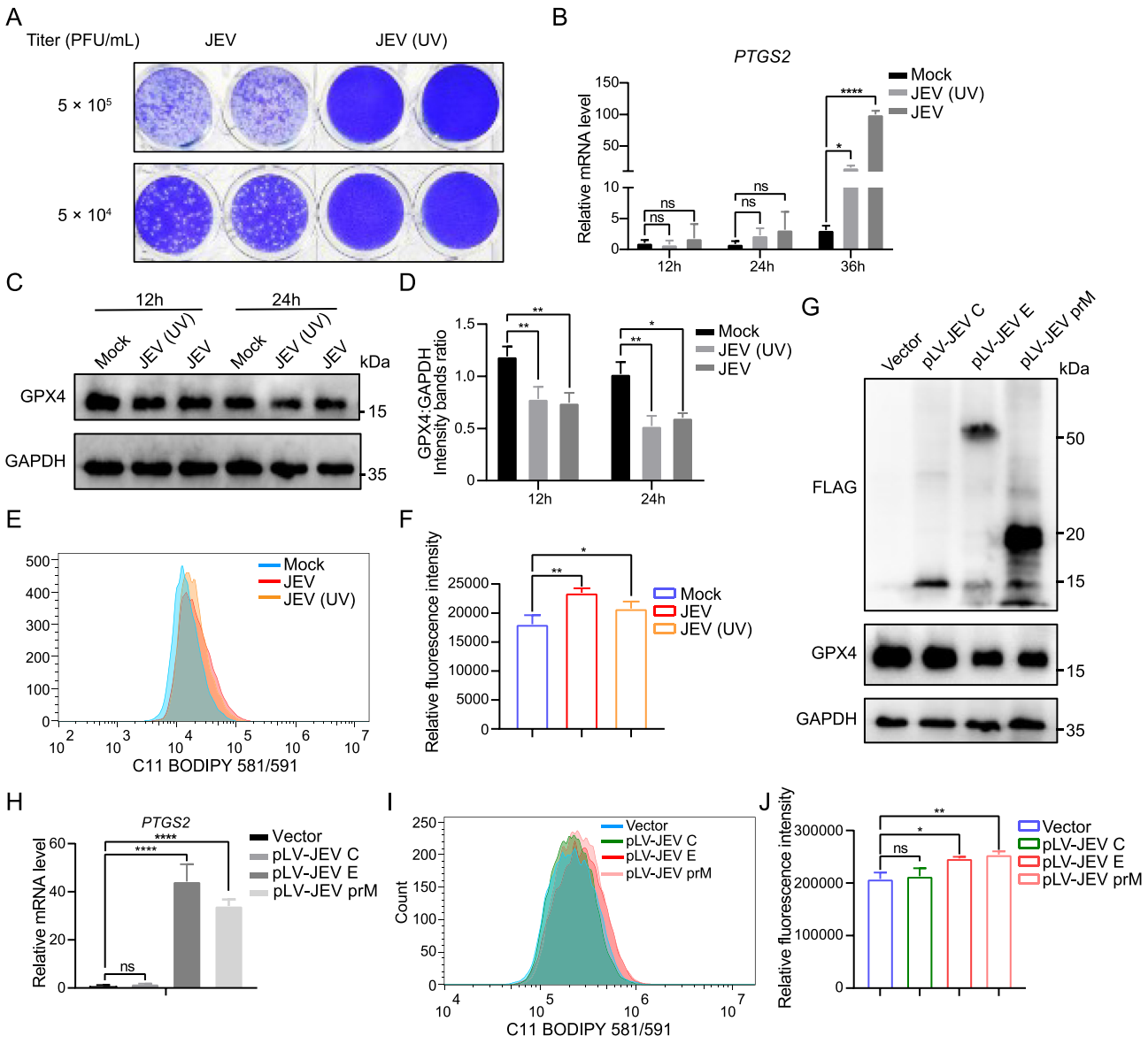

Fig. 4. JEV E and prM proteins contribute to ferroptosis. **A**–**F** SH-SY5Y cells were infected with either UV-inactivated JEV(UV) or JEV at an MOI of 1. The inactivation efficiency was verified through plaque assay (**A**), and the cells were subjected to RT-qPCR to detect the mRNA level of *PTGS2* at indicated time post-infection (**B**). And total proteins were subjected to Western blotting analysis for detecting the expression of GPX4 (**C** and **D**). At indicated time post-infection, the cells were subjected to detect the level of lipid peroxidation (**E** and **F**). (**G to J**) Flag-tagged JEV C, E, and prM proteins were ectopic expressed in SH-SY5Y cells, and cells were subjected to Western blotting analysis for detecting the expression of Flag and GPX4 (**G**). The mRNA levels of *PTGS2* were determined by RT-qPCR (**H**) and the lipid peroxidation was determined by flow cytometry (**I** and **J**). Data are representative of three independent experiments with three biological replicates. Significance was analyzed using one-way ANOVA with Dunnett's multiple comparisons test (**B**, **D**, **F**, **H** and **J**) (n = 3 in each group). $^{*}P < 0.05$, $^{**}P < 0.01$, $^{****}P < 0.0001$. ns, not significant.

Neuronal injury is a powerful physiological trigger for glial activation after JEV infection (Chen et al., 2010). To simulate this process, we then incubated mouse primary glial cells with UV-inactivated supernatant of JEV-infected neurons collected in the previous experiment. It was shown that the Lip-1 treatment obviously weakens the activation of glial cells induced by the supernatant from JEV-infected neurons (Fig. 5C). Taken together, our data demonstrate that inhibition of ferroptosis can not only directly inhibit JEV-induced neuronal inflammatory response, but also indirectly inhibit the activation of glial cells, hinting the key role of ferroptosis in JEV-induced neuroinflammation.

3.6. *Ferroptosis is involved in the pathogenesis of JEV*

To further verify whether JEV infection can lead to ferroptosis *in vivo*, we first tested JEV-infected mouse brains, and found that JEV infection could significantly promote the expression of *Ptgs2* and suppress GPX4 (Supplementary Fig. S4A–C). Moreover, an increased malondialdehyde (MDA) level in brains were observed, which is a lipid peroxidation product (Supplementary Fig. S4D). These results indicate that ferroptosis occurs in the brains of JEV-infected mice. Subsequently, in order to explore the contribution of ferroptosis to the pathogenesis of JEV, a mouse model of JEV infection was employed. Briefly, six-week-old C57BL/6 mice were infected intraperitoneally with 10^5 PFU JEV or with an equal volume of DMEM. The mice were administrated intravenously with Lip-1 at a dose of 10 mg/kg or an equal volume of DMSO once a day for 3 days. The state of mice was continuously observed and recorded until 25 days post-infection, and samples were collected at corresponding time points for subsequent detection (Fig. 6A). As shown in Fig. 6B–C, Lip-1 treatment reduced mortality and ameliorated clinical signs of acute encephalitis in JEV infected mice. Meanwhile, we

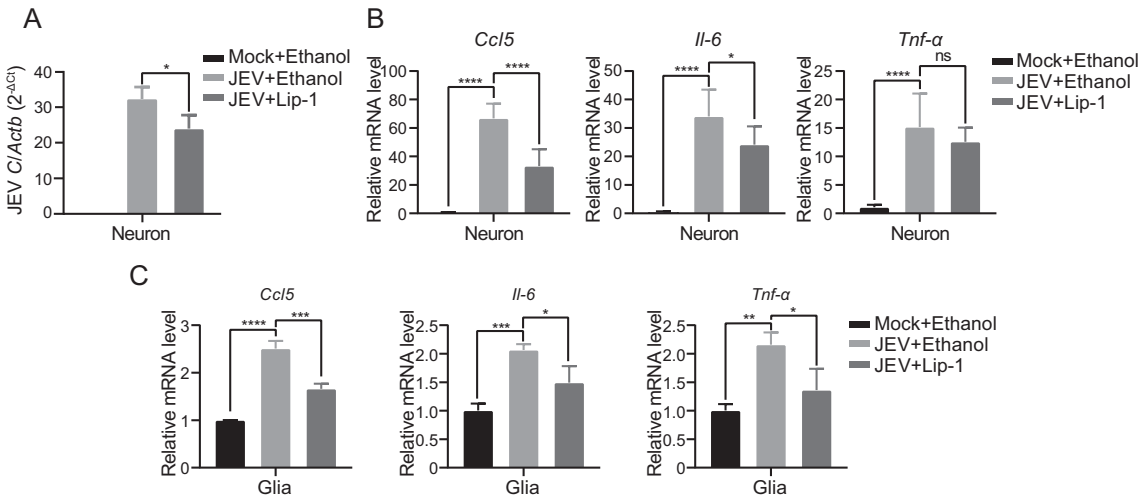

Fig. 5. Ferroptosis contributes to JEV-induced neuroinflammatory response *in vitro*. Primary neurons were infected or mock-infected with JEV at an MOI of 1, followed by incubated with 10 μmol/L Lip-1 or the vehicle (Ethanol). At 48 h post-infection, the supernatant was collected and inactivated by UV treatment. Mouse primary glial cells were incubated with UV-inactivated supernatant of JEV-infected neurons for another 48 h. The primary neurons (**A** to **D**) and glial cells (**E** to **G**) were subjected to RT-qPCR to detect the mRNA level of JEV *C* gene and the proinflammatory genes (*Ccl-5, Il-6, Tnf-α*). Data are representative of three independent experiments with three biological replicates. Significance was analyzed using one-way ANOVA with Dunnett's multiple comparisons test (n = 3 in each group). *$P <$ 0.05, **$P <$ 0.01, **$P <$ 0.001, ****$P <$ 0.0001. ns, not significant.

measured the viral load in the brains of mice from each group at 6 days post-infection, and the results showed that virus titer significantly lower in Lip-1 treated groups (Fig. 6D). These results collectively suggest that the inhibition of ferroptosis reduces the lethality of the JEV-infected mice and reduces the proliferation of JEV in the brain.

Moreover, on the 6th day post-infection, a general histological examination of brains was conducted to evaluate whether ferroptosis is associated with JEV-induce pathological changes. The brain tissue of JEV-infected mice developed vascular sleeves and meningitis, which was mitigated by Lip-1 (Fig. 6E). Excessive inflammatory responses mediated by activated glial cells are known to contribute to the pathogenesis of JEV (Ghoshal et al., 2007). To verify if ferroptosis is involved in this process, we performed IHC experiments with antibodies against IBA-1 and GFAP, which specifically recognizes microglia and astrocytes, and found that Lip-1 treatment reduced the proliferation of microglia and astrocytes in JEV-infected mice (Fig. 6F). Furthermore, inflammatory cytokines in brain tissue were also detected. It was observed that Lip-1 treatment significantly reduced the production of inflammatory cytokines in the brain tissue of JEV-infected mice (Fig. 6G). In summary, these results suggest that ferroptosis is involved in pathogenesis of JEV *in vivo*, and highlight it as a potential therapeutic target for JEV-related diseases.

4. Discussion

Since the discovery of ferroptosis as a form of programmed cell death, a large number of studies have focused on its implications in various diseases, including cancer, neurodegenerative diseases, acute kidney injury and stroke and other diseases (Li et al., 2020). In recent years, relevant literature has explored the relationship between viral infection and ferroptosis, however, the specific connection to the pathogenesis of flavivirus, especially JEV, remained to be further explored. In this study, we demonstrate that ferroptosis is involved in the neuronal death induced by JEV infection *in vivo* and *in vitro*. On the one hand, JEV reduces the activity of GPX4 by reducing the level of GSH, resulting in the loss of antioxidant capacity of neurons, which leads to the occurrence of ferroptosis. On the other hand, JEV infection promotes the expression of ACSL4 through YAP1, hinting that JEV may mediate the production of PUFA through this pathway, thereby interfering with the synthesis of neuronal polyunsaturated lipids and ultimately promoting the occurrence of ferroptosis. Importantly, we found that the inhibition of ferroptosis can reduce neuroinflammation and attenuate brain damage caused by JEV infection. These results indicate that ferroptosis plays an important role in the pathogenesis of JEV, and suggest that targeting ferroptosis may become a new therapeutic method for Japanese encephalitis in the future.

It has been reported that glutamate and oxidative damage may play an important role in neurobehavioral impairment and cell death in JEV-infected rats (Chauhan et al., 2017), and flavivirus infection induces oxidative stress in infected cells (Kumar et al., 2009; Wang et al., 2013; Olagnier et al., 2014), implying that ferroptosis may be involved in the pathogenic process of JEV. Ferroptosis occurs when the rate of intracellular lipid reactive oxygen species production exceeds the oxidative capacity of cells. The main antioxidant system in cells is the system Xc−/GSH/GPX4 axis (Dixon et al., 2012; Friedmann Angeli et al., 2014; Yang et al., 2014), therefore, dysfunction of any one part of this system can lead to the occurrence of ferroptosis. The system Xc− is a cystine/glutamate anti-transporter that promotes the exchange of cystine and glutamate on the plasma membrane (Bannai and Kitamura, 1980), and Cystine is the limiting amino acid for GSH synthesis (Mandal et al., 2010; Doll and Conrad, 2017). Inactivation of GPX4 caused by GSH deficiency will lead to disorder function of cellular antioxidant system and abnormal accumulation of ROS, which promotes the occurrence of lipid peroxidation and causes membrane damage (Maiorino et al., 2018). In this study, we demonstrated that JEV-infection suppresses intracellular antioxidant function by inhibiting GPX4 expression but did not further explore whether JEV also altered the function of systemic Xc−. Given that a previous study has shown that NDV infection can induce ferroptosis by inhibiting the Xc−/GSH/GPX4 axis (Kan et al., 2021), it is reasonable to propose that the regulation of system Xc− may also play a role in JEV-induced ferroptosis cell death. These reports are consistent with our findings, whether JEV infection can affect the function of system Xc−/GSH/GPX4 axis is worth further exploring.

The role of ACSL4 in ferroptosis sensitivity and its contribution to this regulated cell death process have been confirmed by recent studies (Yuan et al., 2016; Kagan et al., 2017; Chen et al., 2021). ACSL4 plays a critical role in the metabolism and incorporation of PUFAs into the phospholipid membranes of cells (Bouchaoui et al., 2022). Esterified PUFAs are particularly susceptible to lipid peroxidation, which initiates the

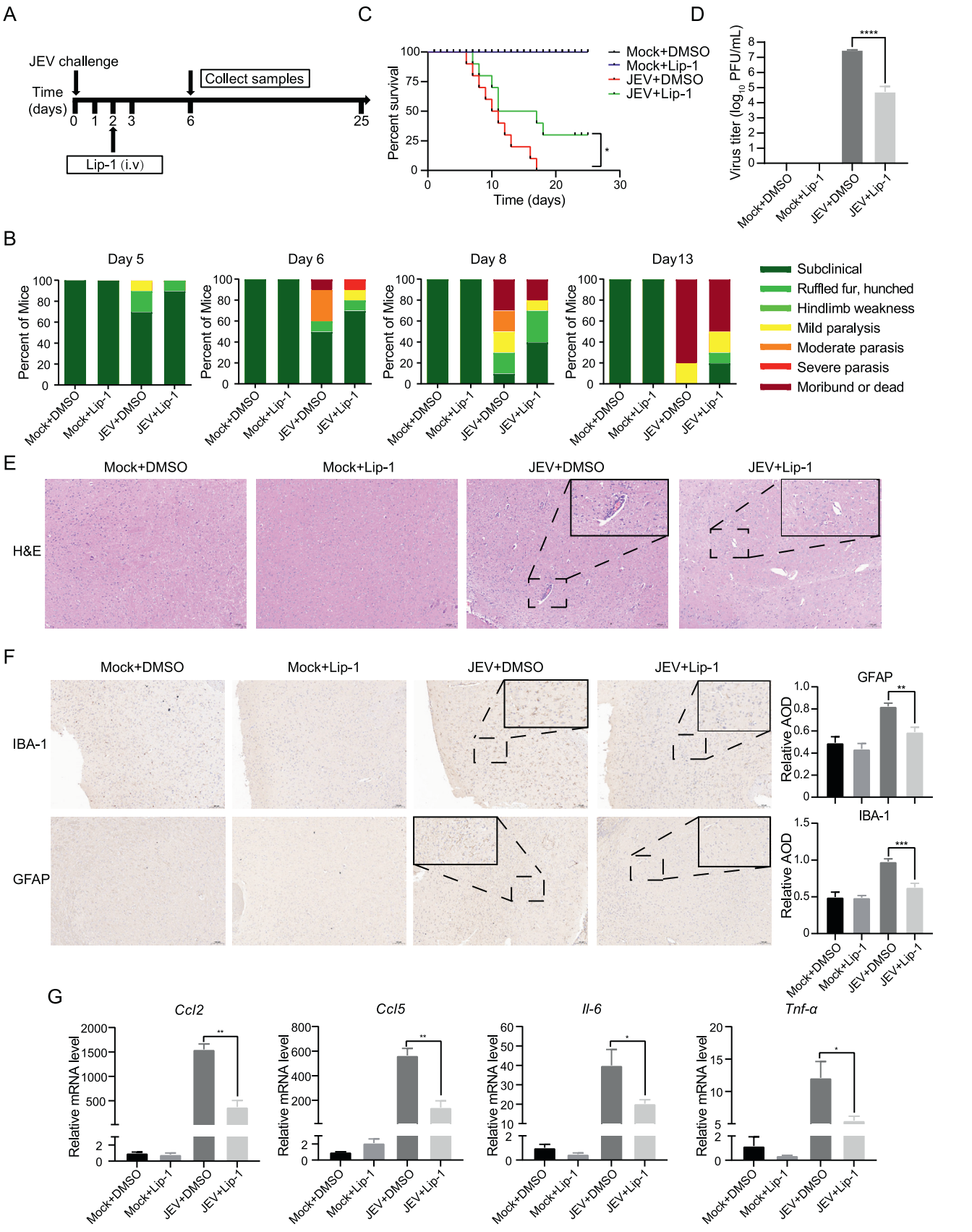

(caption on next page)

Fig. 6. Ferroptosis is involved in JEV pathogenesis *in vivo*. **A** Diagram of infection scheme and subsequent treatment model in animal experiment. Six-week-old C57BL/6 mice (n = 13 per group) were intraperitoneally infected with 10^5 PFU JEV or mock infected, and JEV infected mice were intravenously treated with Lip-1 or DMSO. The mice's condition was continuously observed and recorded until 25 days post-infection, and samples were collected at 6 days post-infection for subsequent detection. **B**–**C** The survival rate and behavioral score of mice in each group were monitored at 25 days post-infection JEV. **D** Viral titers in the mouse brain were detected by plaque assay at 6th day after JEV infection. **E** Pathological changes in mouse brain tissues were analyzed by H&E staining. **F** Immunohistochemistry (IHC) was performed to observe the activation of glial cells or the death of neurons. Black box visualization indicates activated glial cells and perivascular cuffing. Scale bar, 100 μm. An integrated option density analysis of three visual fields from each group was performed to quantify the results of IHC. **G** The mRNA expression levels of inflammatory cytokines (*Ccl2*, *Ccl5*, *Il-6* and *Tnf-α*) in brain tissue lysates were quantified by RT-qPCR. Significance was analyzed using a Student's two-tailed unpaired t-test (**D**, **F** and **G**) (n = 3 in each group), or using survival curve comparison (C), $^*P < 0.05$, $^{**}P < 0.01$, $^{***}P < 0.001$, $^{****}P < 0.0001$.

ferroptosis (Kagan et al., 2020; Yang et al., 2022). More importantly, the fact that the brain is rich in two key ACSL4 substrates, arachidonic acid and docosahexaenoic acid (Chen et al., 2008), prompted us to focus on ACSL4-mediated lipid metabolism pathways in the pathogenesis of JEV. Our results revealed that JEV infection promoted the expression of ACSL4 in neurons, and caused neuronal lipid peroxidation and ferroptosis. Moreover, we also observed a significant upregulation of YAP1 expression in JEV-infected neurons, which is related to the Hippo signaling pathway (Cottini et al., 2014). YAP1 is a transcriptional coactivator that regulates various cellular processes, including ferroptosis (Dai et al., 2020; Sun and Chi, 2021), and it has been reported that YAP mediates exertional heatstroke induced ACSL4 upregulation through TEAD1/TEAD4-related Hippo signaling, which in turn increases lipid peroxidation levels and causes ferroptosis in skeletal muscle cells (Yang et al., 2020; He et al., 2022). Specifically, our results suggest that the oncoprotein YAP1 upregulated the expression of ACSL4 in response to JEV infection, which whereafter promotes the neuronal ferroptosis. It is worth noting that in our study, we found that knockdown of YAP1 significantly decreased the expression of GPX4, a key suppressor of ferroptosis (Fig. 3M). This may be the reason why that the effect of knockdown of YAP1 was not as effective as knockdown of ACSL4 on suppressing JEV-induced ferroptosis, as attenuation of GPX4 restored the inhibitory effect of ferroptosis caused by YAP1 knockdown, while studies have shown knockdown of ACSL4 would promote the expression of GPX4 (Li et al., 2019; Wang et al., 2022). These findings highlight the complexity of the interplay between various signaling pathways and their effects on expression of ACSL4 in JEV-induced ferroptosis and other neurodegenerative diseases.

The most typical clinical feature of JE is extensive inflammation of the brain, and its clinical symptoms and mortality are associated with viral titers in the brain, production of inflammatory mediators, and destruction of the blood-brain barrier (Li et al., 2015). Based on the above finding that JEV infection can induce ferroptosis in neurons, we further explored the role of ferroptosis in JEV-induced neuroinflammation. In our experiments, we utilized the ferroptosis inhibitor Lip-1 and found that it effectively inhibits the replication of JEV, suggesting that the ROS induced by JEV infection may play a significant role in its replication and proliferation. Furthermore, Lip-1 also inhibited the inflammatory response in JEV-infected neurons and microglia cells, and reduced neuroinflammation in JEV-infected mice. These findings suggest that ferroptosis is strongly associated with neuroinflammation induced by JEV infection. Lip-1 has been shown to have therapeutic potential for various diseases. It has been reported to mitigate neurologic deficits and cerebral edema following subarachnoid hemorrhage and to reduce neuronal cell death (Cao et al., 2021). In addition, Lip-1 also prevents steatosis and steatohepatitis in mice with metabolic dysfunction-associated fatty liver disease (Tong et al., 2023). In our study, we administered Lip-1 into JEV-infected mice with tail vein. Therefore, we cannot exclude the possibility that the inhibitor has influenced the pathogenic process of the JEV in the peripheral circulation. Additionally, we only assessed the changes in virus titer within the mouse brain, thus we were unable to determine whether the inhibitor altered the amount of virus entering the brain by affecting viral replication in the periphery. Ultimately, we only detected some widely accepted representative inflammatory factors that can be regulated by JEV infection through RT-qPCR (Wang et al., 2020; Zhu et al., 2023), further studies using other more precise methods such as ELISA to identify more inflammatory factors or chemokines specifically expressed by neurons or glial cells will be beneficial to further elucidate the specific function of ferroptosis in JEV pathogenesis. At the same time, although our study proved that ferroptosis is involved in the pathogenesis of JEV, the contribution of other forms of cell death were ignored. Considering that various inflammatory forms of cell death including necrosis and pyroptosis are involved in the pathogenesis of JEV (Ashraf et al., 2021), accurately finding the inflammatory factors related to ferroptosis will also contribute to explore the potential crosstalk between different cell deaths. Hence, further studies are required to systematically explore the role of ferroptosis in JEV pathogenesis.

5. Conclusion

In summary, our study demonstrates that JEV infection can lead to neuronal ferroptosis by inhibiting the antioxidant function of GSH-GPX4 and promoting ACSL4 mediated lipid peroxidation. Furthermore, we also found that ferroptosis is involved in JEV induced neuroinflammatory responses and cerebral damage, and inhibiting ferroptosis can inhibit JEV induced CNS damage.

Data availability

All data relevant to this study are included in the article or uploaded as supplementary information.

Ethics statement

All animal studies were conducted in strict accordance with the Guide for care and use of Laboratory Animals of Laboratory Animal Centre, Huazhong Agriculture University, and all experiments conform to the relevant regulatory standards. The experiments and protocols were approved by the Animal Management and Ethics Committee of Huazhong Agriculture University (HZAUMO-2023-0042).

Author contributions

Wenjing Zhu: methodology, validation, investigation, data curation, formal analysis, visualization, writing-original draft, and editing. Qi Li: methodology and formal analysis. Yong yin: validation and investigating. Huanchun Chen: methodology. Youhui Si: methodology and formal analysis. Bibo Zhu: methodology. Shengbo Cao: conceptualization and supervision. Zikai Zhao: investigation, validation, writing-original draft, writing-reviewing, and editing. Jing Ye: conceptualization, data curation, formal analysis, funding acquisition, supervision, validation, writing-reviewing, and editing.

Conflict of interest

The authors declare that they have no conflict of interest.

Acknowledgements

This work was supported by National Natural Science Foundation of China (32022082, 31972721), National Key Research and Development Program of China (2022YFD1801500, 2022YFD1800105), Natural Science Foundation of Hubei Province (2021CFA056), and Fundamental Research Funds for the Central Universities (2662023PY005).

Appendix A. Supplementary data

Supplementary data to this article can be found online at https://doi.org/10.1016/j.virs.2023.12.004.

References

Ashraf, U., Ding, Z., Deng, S., Ye, J., Cao, S., Chen, Z., 2021. Pathogenicity and virulence of Japanese encephalitis virus: neuroinflammation and neuronal cell damage. Virulence 12, 968–980.

Bannai, S., Kitamura, E., 1980. Transport interaction of L-cystine and L-glutamate in human diploid fibroblasts in culture. J. Biol. Chem. 255, 2372–2376.

Bouchaoui, H., Mahoney-Sanchez, L., Garcon, G., Berdeaux, O., Alleman, L.Y., Devos, D., Duce, J.A., Devedjian, J.C., 2022. ACSL4 and the lipoxygenases 15/15B are pivotal for ferroptosis induced by iron and PUFA dyshomeostasis in dopaminergic neurons. Free Radic. Biol. Med. 195, 145–157.

Cao, J.Y., Dixon, S.J., 2016. Mechanisms of ferroptosis. Cell. Mol. Life Sci. 73, 2195–2209.

Cao, Y., Li, Y., He, C., Yan, F., Li, J.R., Xu, H.Z., Zhuang, J.F., Zhou, H., Peng, Y.C., Fu, X.J., Lu, X.Y., Yao, Y., Wei, Y.Y., Tong, Y., Zhou, Y.F., Wang, L., 2021. Selective ferroptosis inhibitor liproxstatin-1 attenuates neurological deficits and neuroinflammation after subarachnoid hemorrhage. Neurosci. Bull. 37, 535–549.

Chauhan, P.S., Misra, U.K., Kalita, J., 2017. A study of glutamate levels, NR1, NR2A, NR2B receptors and oxidative stress in rat model of Japanese encephalitis. Physiol. Behav. 171, 256–267.

Chen, C.J., Ou, Y.C., Lin, S.Y., Raung, S.L., Liao, S.L., Lai, C.Y., Chen, S.Y., Chen, J.H., 2010. Glial activation involvement in neuronal death by Japanese encephalitis virus infection. J. Gen. Virol. 91, 1028–1037.

Chen, C.T., Green, J.T., Orr, S.K., Bazinet, R.P., 2008. Regulation of brain polyunsaturated fatty acid uptake and turnover. Prostaglandins Leukot. Essent. Fatty Acids 79, 85–91.

Chen, J., Li, X., Ge, C., Min, J., Wang, F., 2022. The multifaceted role of ferroptosis in liver disease. Cell Death Differ. 29, 467–480.

Chen, X., Li, J., Kang, R., Klionsky, D.J., Tang, D., 2021. Ferroptosis: machinery and regulation. Autophagy 17, 2054–2081.

Cottini, F., Hideshima, T., Xu, C., Sattler, M., Dori, M., Agnelli, L., Ten Hacken, E., Bertilaccio, M.T., Antonini, E., Neri, A., Ponzoni, M., Marcatti, M., Richardson, P.G., Carrasco, R., Kimmelman, A.C., Wong, K.K., Caligaris-Cappio, F., Blandino, G., Kuehl, W.M., Anderson, K.C., Tonon, G., 2014. Rescue of Hippo coactivator YAP1 triggers DNA damage-induced apoptosis in hematological cancers. Nat. Med. 20, 599–606.

Dai, C., Chen, X., Li, J., Comish, P., Kang, R., Tang, D., 2020. Transcription factors in ferroptotic cell death. Cancer Gene Ther. 27, 645–656.

Dixon, S.J., Lemberg, K.M., Lamprecht, M.R., Skouta, R., Zaitsev, E.M., Gleason, C.E., Patel, D.N., Bauer, A.J., Cantley, A.M., Yang, W.S., Morrison 3rd, B., Stockwell, B.R., 2012. Ferroptosis: an iron-dependent form of nonapoptotic cell death. Cell 149, 1060–1072.

Doll, S., Conrad, M., 2017. Iron and ferroptosis: a still ill-defined liaison. IUBMB Life 69, 423–434.

Doll, S., Proneth, B., Tyurina, Y.Y., Panzilius, E., Kobayashi, S., Ingold, I., Irmler, M., Beckers, J., Aichler, M., Walch, A., Prokisch, H., Trumbach, D., Mao, G., Qu, F., Bayir, H., Fullekrug, J., Scheel, C.H., Wurst, W., Schick, J.A., Kagan, V.E., Angeli, J.P., Conrad, M., 2017. ACSL4 dictates ferroptosis sensitivity by shaping cellular lipid composition. Nat. Chem. Biol. 13, 91–98.

Forcina, G.C., Dixon, S.J., 2019. GPX4 at the crossroads of lipid homeostasis and ferroptosis. Proteomics 19, e1800311.

Friedmann Angeli, J.P., Schneider, M., Proneth, B., Tyurina, Y.Y., Tyurin, V.A., Hammond, V.J., Herbach, N., Aichler, M., Walch, A., Eggenhofer, E., Basavarajappa, D., Radmark, O., Kobayashi, S., Seibt, T., Beck, H., Neff, F., Esposito, I., Wanke, R., Forster, H., Yefremova, O., Heinrichmeyer, M., Bornkamm, G.W., Geissler, E.K., Thomas, S.B., Stockwell, B.R., O'donnell, V.B., Kagan, V.E., Schick, J.A., Conrad, M., 2014. Inactivation of the ferroptosis regulator Gpx4 triggers acute renal failure in mice. Nat. Cell Biol. 16, 1180–1191.

Ghoshal, A., Das, S., Ghosh, S., Mishra, M.K., Sharma, V., Koli, P., Sen, E., Basu, A., 2007. Proinflammatory mediators released by activated microglia induces neuronal death in Japanese encephalitis. Glia 55, 483–496.

He, S., Li, R., Peng, Y., Wang, Z., Huang, J., Meng, H., Min, J., Wang, F., Ma, Q., 2022. ACSL4 contributes to ferroptosis-mediated rhabdomyolysis in exertional heat stroke. J. Cachexia Sarcopenia Muscle 13, 1717–1730.

Kagan, V.E., Mao, G., Qu, F., Angeli, J.P., Doll, S., Croix, C.S., Dar, H.H., Liu, B., Tyurin, V.A., Ritov, V.B., Kapralov, A.A., Amoscato, A.A., Jiang, J., Anthonymuthu, T., Mohammadyani, D., Yang, Q., Proneth, B., Klein-Seetharaman, J., Watkins, S., Bahar, I., Greenberger, J., Mallampalli, R.K., Stockwell, B.R., Tyurina, Y.Y., Conrad, M., Bayir, H., 2017. Oxidized arachidonic and adrenic PEs navigate cells to ferroptosis. Nat. Chem. Biol. 13, 81–90.

Kagan, V.E., Tyurina, Y.Y., Sun, W.Y., Vlasova, I.I., Dar, H., Tyurin, V.A., Amoscato, A.A., Mallampalli, R., Van Der Wel, P.C.A., He, R.R., Shvedova, A.A., Gabrilovich, D.I., Bayir, H., 2020. Redox phospholipidomics of enzymatically generated oxygenated phospholipids as specific signals of programmed cell death. Free Radic. Biol. Med. 147, 231–241.

Kan, X.J., Yin, Y.C., Song, C.P., Tan, L., Qiu, X.S., Liao, Y., Liu, W.W., Meng, S.S., Sun, Y.J., Ding, C., 2021. Newcastle-disease-virus-induced ferroptosis through nutrient deprivation and ferritinophagy in tumor cells. iScience 24, 102837.

Khare, B., Kuhn, R.J., 2022. The Japanese encephalitis antigenic complex viruses: from structure to immunity. Viruses 14, 2213.

Kumar, S., Misra, U.K., Kalita, J., Khanna, V.K., Khan, M.Y., 2009. Imbalance in oxidant/antioxidant system in different brain regions of rat after the infection of Japanese encephalitis virus. Neurochem. Int. 55, 648–654.

Lee, H., Zandkarimi, F., Zhang, Y., Meena, J.K., Kim, J., Zhuang, L., Tyagi, S., Ma, L., Westbrook, T.F., Steinberg, G.R., Nakada, D., Stockwell, B.R., Gan, B., 2020. Energy-stress-mediated AMPK activation inhibits ferroptosis. Nat. Cell Biol. 22, 225–234.

Li, F., Wang, Y., Yu, L., Cao, S., Wang, K., Yuan, J., Wang, C., Wang, K., Cui, M., Fu, Z.F., 2015. Viral infection of the central nervous system and neuroinflammation precede blood-brain barrier disruption during Japanese encephalitis virus infection. J. Virol. 89, 5602–5614.

Li, J., Cao, F., Yin, H.L., Huang, Z.J., Lin, Z.T., Mao, N., Sun, B., Wang, G., 2020. Ferroptosis: past, present and future. Cell Death Dis. 11, 88.

Li, Y., Feng, D., Wang, Z., Zhao, Y., Sun, R., Tian, D., Liu, D., Zhang, F., Ning, S., Yao, J., Tian, X., 2019. Ischemia-induced ACSL4 activation contributes to ferroptosis-mediated tissue injury in intestinal ischemia/reperfusion. Cell Death Differ. 26, 2284–2299.

Liu, G.Z., Xu, X.W., Tao, S.H., Gao, M.J., Hou, Z.H., 2021. HBx facilitates ferroptosis in acute liver failure via EZH2 mediated SLC7A11 suppression. J. Biomed. Sci. 28, 67.

Maiorino, M., Conrad, M., Ursini, F., 2018. GPx4, lipid peroxidation, and cell death: discoveries, rediscoveries, and open issues. Antioxid. Redox Signal. 29, 61–74.

Mandal, P.K., Seiler, A., Perisic, T., Kolle, P., Banjac Canak, A., Forster, H., Weiss, N., Kremmer, E., Lieberman, M.W., Bannai, S., Kuhlencordt, P., Sato, H., Bornkamm, G.W., Conrad, M., 2010. System x(c)- and thioredoxin reductase 1 cooperatively rescue glutathione deficiency. J. Biol. Chem. 285, 22244–22253.

Olagnier, D., Peri, S., Steel, C., Van Montfoort, N., Chiang, C., Beljanski, V., Slifker, M., He, Z., Nichols, C.N., Lin, R., Balachandran, S., Hiscott, J., 2014. Cellular oxidative stress response controls the antiviral and apoptotic programs in dengue virus-infected dendritic cells. PLoS Pathog. 10, e1004566.

Stockwell, B.R., Friedmann Angeli, J.P., Bayir, H., Bush, A.I., Conrad, M., Dixon, S.J., Fulda, S., Gascon, S., Hatzios, S.K., Kagan, V.E., Noel, K., Jiang, X., Linkermann, A., Murphy, M.E., Overholtzer, M., Oyagi, A., Pagnussat, G.C., Park, J., Ran, Q., Rosenfeld, C.S., Salnikow, K., Tang, D., Torti, F.M., Torti, S.V., Toyokuni, S., Woerpel, K.A., Zhang, D.D., 2017. Ferroptosis: a regulated cell death nexus linking metabolism, redox biology, and disease. Cell 171, 273–285.

Sun, T., Chi, J.T., 2021. Regulation of ferroptosis in cancer cells by YAP/TAZ and Hippo pathways: the therapeutic implications. Genes Dis. 8, 241–249.

Tang, D., Chen, X., Kang, R., Kroemer, G., 2021. Ferroptosis: molecular mechanisms and health implications. Cell Res. 31, 107–125.

Tong, J., Lan, X.T., Zhang, Z., Liu, Y., Sun, D.Y., Wang, X.J., Ou-Yang, S.X., Zhuang, C.L., Shen, F.M., Wang, P., Li, D.J., 2023. Ferroptosis inhibitor liproxstatin-1 alleviates metabolic dysfunction-associated fatty liver disease in mice: potential involvement of PANoptosis. Acta Pharmacol. Sin. 44, 1014–1028.

Wang, J., Chen, Y., Gao, N., Wang, Y., Tian, Y., Wu, J., Zhang, J., Zhu, J., Fan, D., An, J., 2013. Inhibitory effect of glutathione on oxidative liver injury induced by dengue virus serotype 2 infections in mice. PLoS One 8, e55407.

Wang, Y., Zhang, M., Bi, R., Su, Y., Quan, F., Lin, Y., Yue, C., Cui, X., Zhao, Q., Liu, S., Yang, Y., Zhang, D., Cao, Q., Gao, X., 2022. ACSL4 deficiency confers protection against ferroptosis-mediated acute kidney injury. Redox Biol. 51, 102262.

Wang, Z.Y., Zhen, Z.D., Fan, D.Y., Qin, C.F., Han, D.S., Zhou, H.N., Wang, P.G., An, J., 2020. Axl deficiency promotes the neuroinvasion of Japanese encephalitis virus by enhancing IL-1alpha production from pyroptotic macrophages. J. Virol. 94, e00602-20.

Wu, J., Minikes, A.M., Gao, M., Bian, H., Li, Y., Stockwell, B.R., Chen, Z.N., Jiang, X., 2019. Intercellular interaction dictates cancer cell ferroptosis via NF2-YAP signalling. Nature 572, 402–406.

Xu, X.Q., Xu, T., Ji, W., Wang, C., Ren, Y., Xiong, X., Zhou, X., Lin, S.H., Xu, Y., Qiu, Y., 2022. Herpes simplex virus 1-induced ferroptosis contributes to viral encephalitis. mBio 14, e0237022.

Yagoda, N., Von Rechenberg, M., Zaganjor, E., Bauer, A.J., Yang, W.S., Fridman, D.J., Wolpaw, A.J., Smukste, I., Peltier, J.M., Boniface, J.J., Smith, R., Lessnick, S.L., Sahasrabudhe, S., Stockwell, B.R., 2007. RAS-RAF-MEK-dependent oxidative cell death involving voltage-dependent anion channels. Nature 447, 864–868.

Yan, Q., Zheng, W., Jiang, Y., Zhou, P., Lai, Y., Liu, C., Wu, P., Zhuang, H., Huang, H., Li, G., Zhan, S., Lao, Z., Liu, X., 2023. Transcriptomic reveals the ferroptosis features of host response in a mouse model of Zika virus infection. J. Med. Virol. 95, e28386.

Yang, W.H., Huang, Z., Wu, J., Ding, C.C., Murphy, S.K., Chi, J.T., 2020. A TAZ-ANGPTL4-NOX2 axis regulates ferroptotic cell death and chemoresistance in epithelial ovarian cancer. Mol. Cancer Res. 18, 79–90.

Yang, W.S., Sriramaratnam, R., Welsch, M.E., Shimada, K., Skouta, R., Viswanathan, V.S., Cheah, J.H., Clemons, P.A., Shamji, A.F., Clish, C.B., Brown, L.M., Girotti, A.W., Cornish, V.W., Schreiber, S.L., Stockwell, B.R., 2014. Regulation of ferroptotic cancer cell death by GPX4. Cell 156, 317–331.

Yang, Y., Zhu, T., Wang, X., Xiong, F., Hu, Z., Qiao, X., Yuan, X., Wang, D., 2022. ACSL3 and ACSL4, distinct roles in ferroptosis and cancers. Cancers (Basel) 14, 5896.
Yuan, H., Li, X.M., Zhang, X.Y., Kang, R., Tang, D.L., 2016. Identification of ACSL4 as a biomarker and contributor of ferroptosis. Biochem. Biophys. Res. Commun. 478, 1338–1343.
Yuan, H., Pratte, J., Giardina, C., 2021. Ferroptosis and its potential as a therapeutic target. Biochem. Pharmacol. 186, 114486.
Zhang, D., Wu, X., Xue, X., Li, W., Zhou, P., Lv, Z., Zhao, K., Zhu, F., 2023. Ancient dormant virus remnant ERVW-1 drives ferroptosis via degradation of GPX4 and SLC3A2 in schizophrenia. Virol. Sin. https://doi.org/10.1016/j.virs.2023.09.001.
Zhang, H.L., Hu, B.X., Li, Z.L., Du, T., Shan, J.L., Ye, Z.P., Peng, X.D., Li, X., Huang, Y., Zhu, X.Y., Chen, Y.H., Feng, G.K., Yang, D., Deng, R., Zhu, X.F., 2022. PKCbetaII phosphorylates ACSL4 to amplify lipid peroxidation to induce ferroptosis. Nat. Cell Biol. 24, 88–98.
Zhou, H., Zhou, Y.L., Mao, J.A., Tang, L.F., Xu, J., Wang, Z.X., He, Y., Li, M., 2022. NCOA4-mediated ferritinophagy is involved in ionizing radiation-induced ferroptosis of intestinal epithelial cells. Redox Biol. 55, 102413.
Zhu, S., Tao, M., Li, Y., Wang, X., Zhao, Z., Liu, Y., Li, Q., Li, Q., Lu, Y., Si, Y., Cao, S., Ye, J., 2023. H3K27me3 of Rnf19a promotes neuroinflammatory response during Japanese encephalitis virus infection. J. Neuroinflammation 20, 168.